

Article

Nonlinear Multi-Frequency Dynamics of Wind Turbine Components with a Single-Mesh Helical Gear Train

Nkongho Ayuketang Arreyndip ^{1,2,3,*} , Alain Moise Dikande ^{1,2,4} and Ebobenow Joseph ¹

¹ Department of Physics and Applied Physics, University of Buea, Buea 63, Cameroon; dikande.alain@ubuea.cm (A.M.D.); ebobenow@gmail.com (E.J.)

² African Institute for Mathematical Science (AIMS), Limbe 608, Cameroon

³ Polytechnic, Saint Jerome Catholic University of Douala, Douala 5949, Cameroon

⁴ Laboratory of Research on Advance Materials and Non-linear Sciences (LaRaManS), Department of Physics and Applied Physics, University of Buea, Buea 63, Cameroon

* Correspondence: ayuketang@aims-cameroon.org

Received: 12 January 2018; Accepted: 24 February 2018; Published: 1 March 2018

Abstract: A complex nonlinear model for a single-mesh helical gear train is developed by including a time-varying mesh stiffness, axial vibrations, torsional vibrations, shaft and bearing damping, generator back EMF (Electromotive Force) and gear backlashes. With the help of a time series and Fast Fourier Transform (FFT) frequency spectrum, the effects of these nonlinear terms on the wind turbine and generator rotational speeds are studied under different excitation conditions by numerically integrating the associated equations using the RK4 algorithm. Results show that for lightly damped oscillations, an extra harmonic is induced in the generator dynamics due to contributions from internal excitations. However, this extra vibration can be suppressed at higher damping. Big helical angles will generally induce heavy nonlinear vibrations in the turbine and generator; a smaller mesh frequency will induce extra noise in the generator; and the external excitation due to wind gust has a greater influence on the nonlinearity of the wind turbine dynamics as compared to the internal excitations due to static transmission errors, time-varying mesh stiffness and the generator back EMF.

Keywords: nonlinear; single-mesh; dynamics

1. Introduction

1.1. Background

A wind turbine interacting with wind speed undergoes different mechanical dynamics. Some of these dynamics are: tower vibration, torsional dynamics, axial vibrations and a 3p effect, which is usually caused by a non-homogeneous wind speed across the turbine rotor plane and the presence of a tower [1]. These vibrations greatly affect the efficiency of the wind turbine and the generator. Therefore, it is worthwhile and necessary to study them. According to [2], a wind turbine drive train can be seen as a multi-mass system consisting of three inertias, which include the generator rotor, the turbine hub and the blades. Different structural models of a wind turbine drive train have been studied by most researchers, which include the primitive two-mass model. The two-mass model [3] has two inertias that are connected to each other through a spring where the spring represents low stiffness of the drive-train shaft. This model of the drive train has two flexible points, which are: the flexible blades with flexibility located at the blade tip and blade root and the gear box shafts [1]. The first mass consists of the blade tip, and the second consists of the blade root, the hub and the low and high speed shaft of the turbine. The main challenge of adopting this model is that the blade breaking point is rarely provided by manufacturers [1]. Researchers of this model realize that there is a greater need

to consider more sophisticated models as this model fails to address the actual behavior of the wind turbine at the gear stage and only considers the entire gearbox as a gain that adds up to the speed of a high speed shaft.

The multi-mass drive train model has serious drawbacks as it induces multiple torsional modes. Higher torsional modes are also present due to self-oscillation of the hub and generator [1–3]. Moreover, this model presents the blades as flexible with the flexibility associated with the bending effects of the blades that acts symmetrically in the rotor plane and collinear with the shaft torque [1–5]. As far as stability is concerned, this model of the drive train is difficult to stabilize compared to the two-mass model as the system becomes more complex.

So far, there is not yet a mathematical model that can completely describe with accuracy the dynamical behavior of a wind turbine drive train due to complex multi-torsional modes. Therefore, our main focus in this work is to develop a nonlinear multi-mass mathematical model of the drive train with a single helical gear stage to study the effects of tower vibrations, tower-induced vibrations in the drive train and the effect of wind gust on the generator and turbine rotational speeds.

1.2. Literature Survey

To better describe the dynamic behavior of wind turbine components, different wind turbine multi-mass models of the drive train have been studied: Mingming Zhao et al. studied the torsional vibrations of a wind turbine gearbox having two planetary gear stages and one parallel gear stage [4]. They developed a nonlinear model for this gearbox by including a time-varying mesh stiffness, damping, static transmission error and gear backlash. They also considered the external excitation due to wind gust and the internal excitation due to static transmission error. By making use of the time history, FFT spectrum, phase portrait, Poincare map and Lyapunov exponent, they found that the external excitation has the most influence on the torsional vibrations of the wind turbine gearbox components. The mesh stiffness, being another significant factor, has more influence than the other internal excitation sources. The static transmission error has the least influence. In another paper, Mingming Zhao et al. studied a four-degree-of-freedom (DOF) dynamic model of a gearbox using a similar approach [5]. Their approach in this work explains under which conditions the fretting corrosion, as one of the wind turbine gearbox failure modes, may occur. Fuchun Yang et al. [6] also developed and studied a nonlinear dynamic behavior and load sharing model of double-mesh helical gear trains by also including torsional vibration, axial vibration, time-varying mesh stiffness and backlashes. Their results show that there are linear and nonlinear areas in the frequency responses of the system. Jan Helsen et al. also model the wind turbine gearbox by means of three more complex modeling techniques of varying complexity: a purely torsional, rigid six degrees of freedom with discrete flexibility and a flexible multibody technique [7]. Through a non-linear finite element method, which is extended by multi-body system functionalities and aerodynamics based on the blade element momentum theory, the dynamic loads of wind turbine power trains, with particular emphasis on planetary gearbox loads, has also been studied [8]. Many more interesting research has been carried out on the gearbox structure and, in general, the dynamics of multi-body systems [9–12].

1.3. Contribution of This Study

Helical gears have been widely studied and found suitable to use in many mechanical transmission systems because of their advantages such as high carrying capacity, smooth transmission and rare tooth interference [6]. In this work, we will also adopt the helical gear and, in addition to the existing models, consider one of the most important factor of the internal excitation that has rarely been considered, which is the generator back EMF (Electromotive Force). Many researchers have focused more on modeling the gearbox and studying its dynamics. However, in this work, we will study the effects of nonlinear coupling at the gear stage on the wind turbine and generator dynamics.

Therefore, the complete nonlinear model of our six-Degree-Of-Freedom (DOF) system will include torsional vibrations, axial vibrations, time-varying mesh stiffness, shaft and bearing dampings,

generator back EMF and backlashes, with the purpose of studying the characteristics of nonlinear dynamical responses, analyzing the influences of the parameters on the frequency responses.

1.4. Organization of the Paper

The work is divided as follows: in Section 2, we present our model of the drive train, the nonlinear terms and derive the associated equations. Section 3 presents the results from the numerical simulation and discussions, then we end with the conclusions.

2. Methods

In this section, we consider a single-mesh helical gear train shown in Figure 1, which is a common model used to design most wind turbines. If we consider a non-rigid shaft, Figure 2 is an illustrated diagram showing damping and torsional factors attached to each inertia. Contrary to the two-mass model, here, the inertia of the gear wheels is non-negligible. Axial vibrations are constrained by the bearing damping and torsional factors. If motion is constrained only in two dimensions, there are six generalized coordinates $(\theta_1, \theta_2, \theta_3, \theta_4, x_1, x_2)$ associated with the six degrees of freedom; where $\theta_1, \theta_2, \theta_3$ and θ_4 are the angular positions of the turbine, first gear wheel, second gear wheel and generator, respectively, and x_1 and x_2 are the axial displacements of the first and second gear wheels, respectively. The other nonlinear terms are as follows.

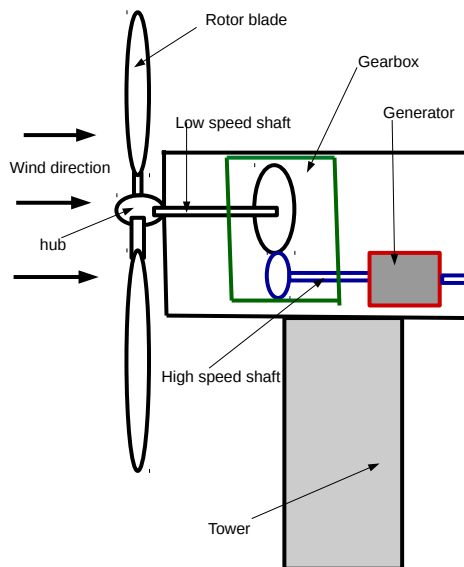


Figure 1. Single-mesh gearbox structure.

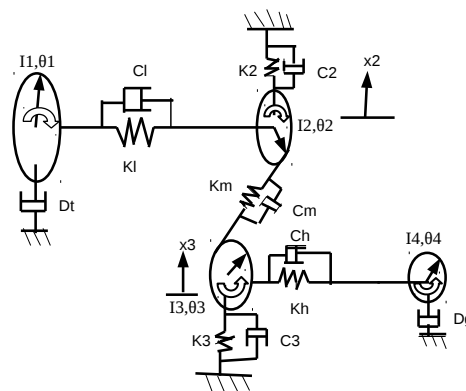


Figure 2. Model of gearbox.

2.1. Mesh Stiffness

The time-varying mesh stiffness is given by [13]:

$$K_m(t) = K_m(0) + K_0(\sin(2\pi f_m t))^2 \tag{1}$$

where $K_m(0)$ is the mesh average stiffness [14], K_0 is the amplitude of the fluctuating term and f_m the mesh frequency.

Another important component of the internal excitation is the static transmission error given by [4,5,15]:

$$e_i(t) = e_0 \sin(w_i t) \tag{2}$$

where e_0 is the small amplitude of the static transmission error and w_i its frequency. The static transmission error in this work is considered to be very small such that only the fluctuating term exists at very low amplitude. Figure 3 is the time series of the mesh stiffness and its Fast Fourier Transform frequency (FFT) spectrum showing the nature of the internal excitation.

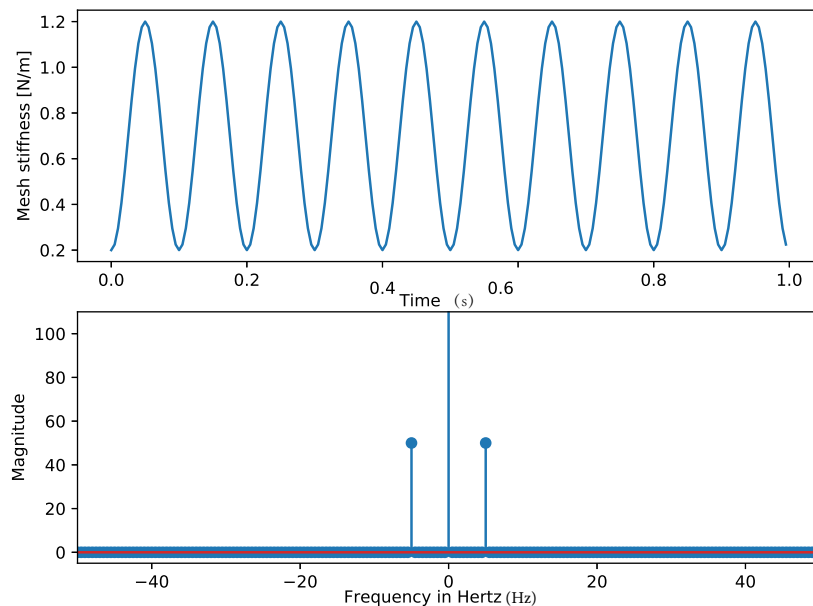


Figure 3. Time-dependent mesh stiffness with its frequency spectrum.

2.2. External Excitation

As the wind drift velocity varies across the wind turbine blades, the torque will also vary. Here, this fluctuation in wind speed, also known as wind gust, is considered sinusoidal given by [4,15]:

$$T_t(t) = T_1 + T_0 \sin(2\pi f_i t) \tag{3}$$

where T_0 and f_i are the amplitude and frequency of the external excitation and T_1 is the average torque due to incoming wind given by:

$$T_1 = \frac{\rho_{air} \pi r_1^2 v^3 C_p}{2\dot{\theta}_1} \tag{4}$$

where ρ_{air} is the air density, r_1 the radius of wind blades, v incoming wind speed, C_p power coefficient and $\dot{\theta}_1$ the rotational speed of the wind turbine. Figure 4 is the time series of the external excitation due to wind gust and its Fast Fourier Transform frequency (FFT) spectrum showing the nature of the excitation.

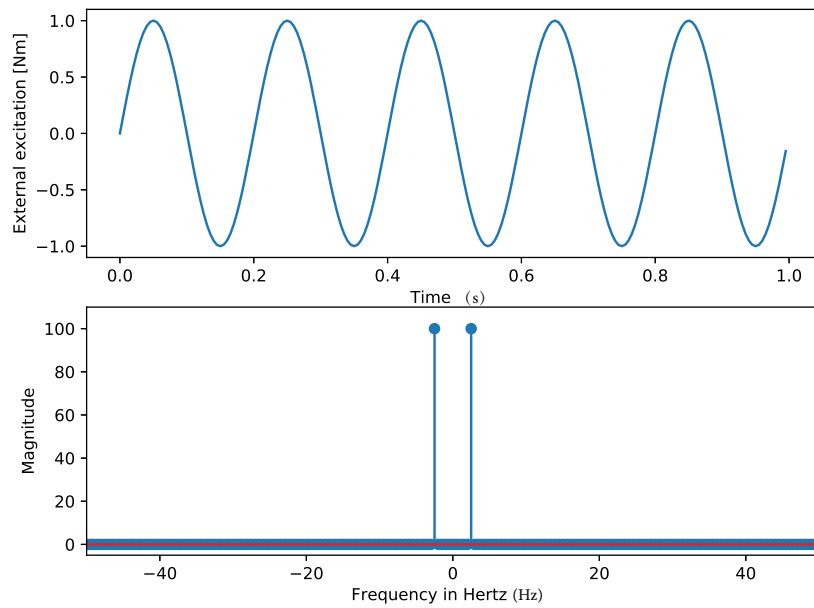


Figure 4. Fluctuating excitation and its frequency spectrum.

2.3. Generator Torque Equation

Here, instead of considering the generator torque to be a constant, we consider it to be periodically varying with the generator angular position. With the periodic motion induced by the back EMF of the generator. The expression is of the form:

$$T_m(t) = T_{m0} + T_j \sin(\omega_j t) \tag{5}$$

where T_{m0} is the average generator torque, T_j is the amplitude and ω_j is the angular frequency of the induced back EMF.

2.4. Backlash Equation

The nonlinear backlash term is given as [4–6],

$$f(u_i) = \begin{cases} u_i - \sigma, & u_i > \sigma \\ 0, & -\sigma < u_i < \sigma \\ u_i + \sigma, & u_i < -\sigma \end{cases} \tag{6}$$

where u_i is the mesh displacement and σ is the half backlash between the contact teeth, with u_i given by:

$$u = \theta_2 r_2 \cos(\beta) + \theta_3 r_3 \cos(\beta) + x_1 \sin(\beta) - x_2 \sin(\beta) \tag{7}$$

where θ_1 and θ_2 are the angular positions of the first and second gear wheels, respectively, r_1 and r_2 are the radii of the first and second gear wheels, respectively, and β is the helical or pressure angle.

2.5. Rotational Equations of Motion

For the rotational degrees of freedom, the rotational equations of motions for the turbine, first and second gear wheels and generator are given respectively by,

$$I_1 \ddot{\theta}_1 = T_t(t) - K_l(\theta_1 - \theta_2) - C_l(\dot{\theta}_1 - \dot{\theta}_2) - D_t \dot{\theta}_1 \tag{8}$$

$$I_2 \ddot{\theta}_2 = K_l(\theta_1 - \theta_2) + C_l(\dot{\theta}_1 - \dot{\theta}_2) - r_2(C_m f'(u) + K_m(t)f(u)) \cos(\beta) \tag{9}$$

$$I_3\ddot{\theta}_3 = -K_h(\theta_3 - \theta_4) - C_h(\dot{\theta}_3 - \dot{\theta}_4) - r_3(C_m f'(u) + K_m(t)f(u)) \cos(\beta) \tag{10}$$

$$I_4\ddot{\theta}_4 = -T_m(t) + K_h(\theta_3 - \theta_4) + C_h(\dot{\theta}_3 - \dot{\theta}_4) - D_t\dot{\theta}_4 \tag{11}$$

where I_1, I_2, I_3 and I_4 are the moment of inertias of the turbine, first and second gear wheels and generator, respectively. $T_t(t)$ is the time-varying external torque; $T_m(t)$ is the time-varying generator torque; and D_t and D_g are turbine and generator damping, respectively. K_l and C_l are low speed shaft torsional and damping constants, respectively; K_h and C_h are high speed shaft torsional and damping constants, respectively; and $K_m(t)$ and C_m time-varying mesh stiffness and damping constants, respectively.

2.6. Equations for Axial Vibrations

For translational degree of freedom, the translational equations of motion of the first and second gear wheels are given respectively by,

$$m_2\ddot{x}_2 = -k_2x_2 - c_2\dot{x}_2 - r_2(C_m f'(u) + K_m(t)f(u)) \sin(\beta) \tag{12}$$

$$m_3\ddot{x}_3 = -k_3x_3 - c_3\dot{x}_3 + r_3(C_m f'(u) + K_m(t)f(u)) \sin(\beta) \tag{13}$$

The above six-degree-of-freedom system can be reduced to four degrees of freedom by imposing a new constraint, which we consider here to be the case where the gear wheels do not slip during the axial vibration; hence, only rotation is allowed. We then consider:

$$x_2 = r_2\theta_2 \tag{14}$$

and:

$$x_3 = r_3\theta_3 \tag{15}$$

where x_2, x_3 are the axial displacements, r_2 and r_3 are the radii of the first and second gear wheels, k_2 and c_2 are the bearing stiffness and damping constants for the first gear wheel and k_3 and c_3 are the bearing stiffness and damping constants for the second gear wheel. Differentiating Equations (14) and (15) twice, substituting into Equations (12) and (13) and adding the results with Equations (9) and (10), the four-degree-of-freedom equations become:

$$\ddot{\theta}_1 = \frac{T_t(t)}{I_1} - \frac{K_l}{I_1}(\theta_1 - \theta_2) - \frac{C_l}{I_1}(\dot{\theta}_1 - \dot{\theta}_2) - \frac{D_t}{I_1}\dot{\theta}_1 \tag{16}$$

$$\ddot{\theta}_2 = \beta_1\theta_1 - \beta_2\theta_2 + \alpha_1\dot{\theta}_1 - \alpha_2\dot{\theta}_2 - \delta_1(C_m f'(u) + K_m(t)f(u))(\cos(\beta) + \sin(\beta)) \tag{17}$$

$$\ddot{\theta}_3 = \beta_3\theta_4 - \beta_4\theta_3 + \alpha_3\dot{\theta}_4 - \alpha_4\dot{\theta}_3 - \delta_2(C_m f'(u) + K_m(t)f(u))(\cos(\beta) + \sin(\beta)) \tag{18}$$

$$\ddot{\theta}_4 = \frac{T_m(t)}{I_4} - \frac{K_h}{I_4}(\theta_4 - \theta_3) - \frac{C_h}{I_4}(\dot{\theta}_4 - \dot{\theta}_3) - \frac{D_g}{I_4}\dot{\theta}_4 \tag{19}$$

where $\beta_1 = K_l/(I_2 + m_2r_2)$, $\beta_2 = (K_l + k_2r_2)/(I_2 + m_2r_2)$, $\alpha_1 = C_l/(I_2 + m_2r_2)$, $\alpha_2 = (C_l + c_2r_2)/(I_2 + m_2r_2)$, $\delta_1 = r_2/(I_2 + m_2r_2)$ and $\beta_3 = K_h/(I_3 + m_3r_3)$, $\beta_4 = (K_h + k_3r_3)/(I_3 + m_3r_3)$, $\alpha_3 = C_h/(I_3 + m_3r_3)$, $\alpha_4 = (C_h + c_3r_3)/(I_3 + m_3r_3)$, $\delta_2 = r_3/(I_3 + m_3r_3)$.

In the nondimensional form, the equations are solved by making the transformation:

$$\tau = \omega t \tag{20}$$

The above set of equations is solved using the RK4 algorithm with the parameter specifications presented in Tables 1 and 2.

Table 1. Table of parameters for Figures 5 and 6.

Name	
Parameters	Values
Inertia (Kgm ²)	$I_1 = I_2 = I_3 = I_4 = 0.09$
mass	$m_1 = m_2 = m_3 = m_4 = 2.0$
Radius	$r_1 = r_2 = 1.0, r_3 = r_4 = 0.2$
Pressure angle	$\beta = \pi/6$
Torsional stiffness	$K_l = 1.0, K_h = 0.01,$
	$K_2 = K_3 = 0.005$
Damping	$C_l = 0.05, C_h = 0.009,$
	$C_2 = C_3 = 0.01,$
	$C_m = 0.001, D_t = 0.01, D_r = 0.009$
Torque	$T(0) = 50.0, T_m(0) = 5.0$
Excitation frequencies	$\omega_i = 0.2, \omega_m = 0.5$

Table 2. Table of parameters for Figures 7–10.

Name	
Parameters	Values
Inertia (Kgm ²)	$I_1 = I_2 = I_3 = I_4 = 0.09$
mass	$m_1 = m_2 = m_3 = m_4 = 2.0$
Radius	$r_1 = r_2 = 1.0, r_3 = r_4 = 0.2$
Torsional stiffness	$K_l = 10.0, K_h = 0.1,$
	$K_2 = K_3 = 0.05$
Damping	$C_l = 0.5, C_h = 0.09,$
	$C_2 = C_3 = 0.1,$
	$C_m = 0.01, D_t = 0.1, D_r = 0.09$
Torque	$T(0) = 50.0, T_m(0) = 5.0$
Excitation frequencies	$\omega_i = 0.2, \omega_m = 0.5$

3. Results and Discussion

In Figures 5 and 6, we investigate the effect of varying the damping and torsional stiffness on the rotational speeds of both the wind turbine and generator, respectively. Figure 5a,b is the time series and frequency response spectrum of wind turbine rotational speed, respectively, at very low damping and torsional constants. Here, we see that multiple values and an amplitude jump exist in the frequency response, which are typical characteristics of nonlinear vibrations. In Figure 5c,d, the damping and torsional terms have been increased by a factor of 10. Here, we see a decrease in the degree of nonlinear vibration at a low amplitude jump. The time series also show highly damped, quasi-periodic vibrations. Hence, the vibrational effect of a wind turbine gearbox components can greatly be controlled by including damping, such as shock absorbers. The effect of higher damping and torsional stiffness is clearly visible in the generator time series and frequency spectrum. In Figure 6a, the time series shows double-periodic vibrations with the system stabilizing at some point in time, and in Figure 6b, two distinct double peaks corresponding to double-periodic oscillations are visible in the frequency spectrum, which could be a result of the fact that the low damping terms failed to suppress the influence of internal excitations on the natural frequency of oscillation of the generator. Hence, extra harmonics are induced. The physical significance is that this can account for a faulty gearbox, and therefore, it should be maintained or replaced. Figure 6c,d shows a reduction of this stochastic vibration at higher damping and torsional constants.

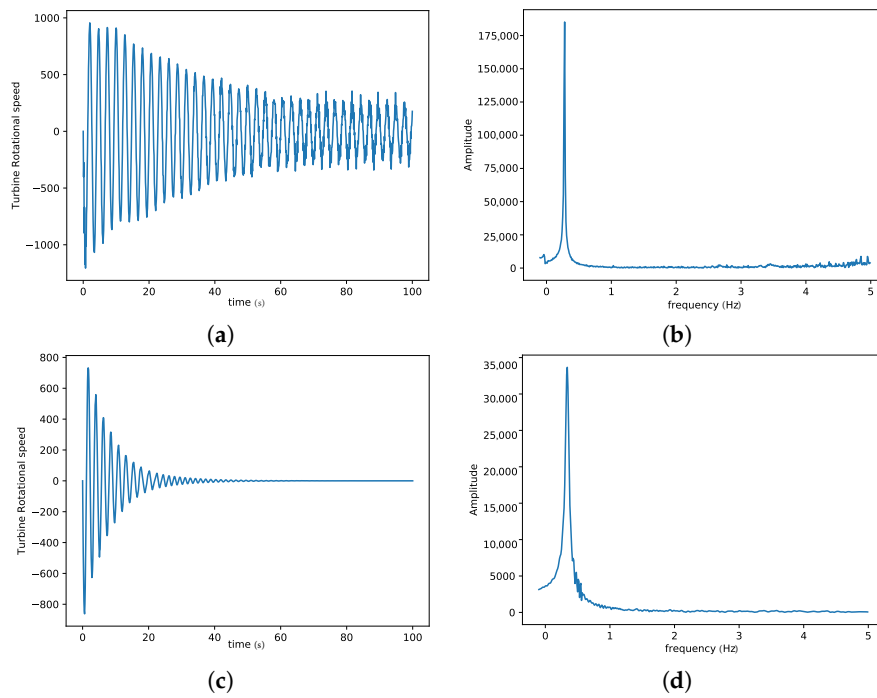


Figure 5. A plot of wind turbine rotational speed ($\dot{\theta}_1$) vs. time (t) to study the effect of higher damping and torsional stiffness. (a,b) are the time series and the corresponding FFT frequency spectrum plots for low damping and torsional stiffness at $K_l = 1.0$, $K_h = 0.01$, $K_2 = K_3 = 0.005$, $C_l = 0.05$, $C_h = 0.009$, $C_2 = C_3 = 0.01$, $C_m = 0.001$, $D_t = 0.01$, $D_g = 0.009$ and $\beta = \pi/6$. In (c,d), the damping and torsional terms have been increased by a factor of 10.

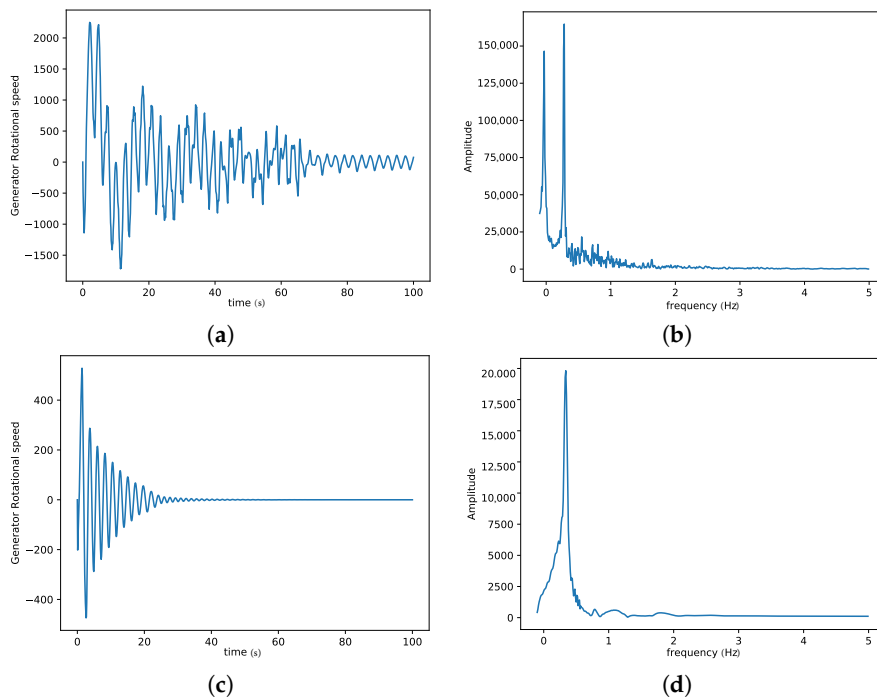


Figure 6. A plot of generator rotational speed ($\dot{\theta}_4$) vs. time (t) to study the effect of higher damping and torsional stiffness. (a,b) are the time series and the corresponding FFT frequency spectrum plots for low damping and torsional stiffness at $K_l = 1.0$, $K_h = 0.01$, $K_2 = K_3 = 0.005$, $C_l = 0.05$, $C_h = 0.009$, $C_2 = C_3 = 0.01$, $C_m = 0.001$, $D_t = 0.01$, $D_g = 0.009$ and $\beta = \pi/6$. In (c,d), the damping and torsional terms have been increased by a factor of 10. The remaining parameters are fixed and presented in Table 1.

In Figures 7 and 8, we study the effect of variation in the helical angle on the wind turbine and generator rotational speed. Figure 7a,b is the time series and frequency spectrum for the case where $\beta = \pi/6$ and Figure 7c,d is for the case where $\beta = \pi/12$. Both the time series and the frequency spectrum show that heavy nonlinear vibrations come with a bigger helical angle, which might lead to tooth separation at the gear stage. A small helical angle has also been seen to induce additional vibration in the turbine that can be seen by the double peak in the frequency spectrum. While the turbine dynamics show that a bigger helical angle can induce heavy nonlinear vibrations, the generator dynamics of Figure 8 show that small helical angles induce more stochastic vibrations, but also become heavily nonlinear at higher helical angles.

In Figure 9, we study the effect of variation in the mesh frequency on the turbine and generator rotational speed using only the frequency spectrum. Figure 9a,b is the turbine and generator frequency response at $w_m = 0.05$ Hz, respectively. Figure 9c,d is the turbine and generator frequency responses at $w_m = 0.5$ Hz. Here, we see that the generator frequency response shows higher, nonlinear stochastic dynamics at lower mesh frequency than at higher mesh frequency, but has very little effect on the turbine dynamics.

Figure 10 is the study of the effect of variation in the frequency of the external excitation on the wind turbine dynamics. Figure 10a is for the case $w_i = 0.02$ Hz, and Figure 10b is for the case $w_i = 0.2$ Hz. Here, we see that an increase in the frequency of the external excitation has a greater influence on the nonlinear vibration of the wind turbine as the frequency response becomes more nonlinear at higher external frequencies.

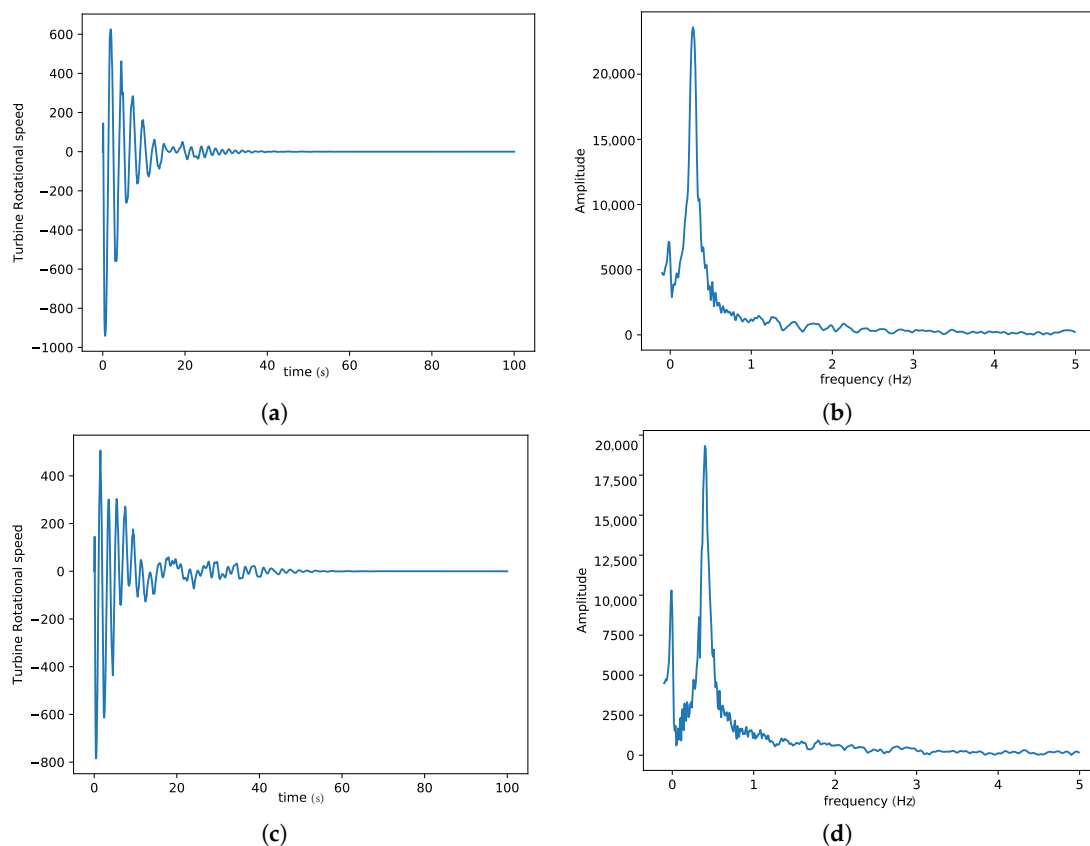


Figure 7. The effect of a bigger helical angle on wind turbine rotational speed ($\dot{\theta}_1$). (a,b) are the time series and the corresponding FFT frequency spectrum plots for the case $\beta = \pi/6$. In (c,d), the helical angle has been set to $\beta = \pi/12$. The other parameters are fixed and listed in Table 2.

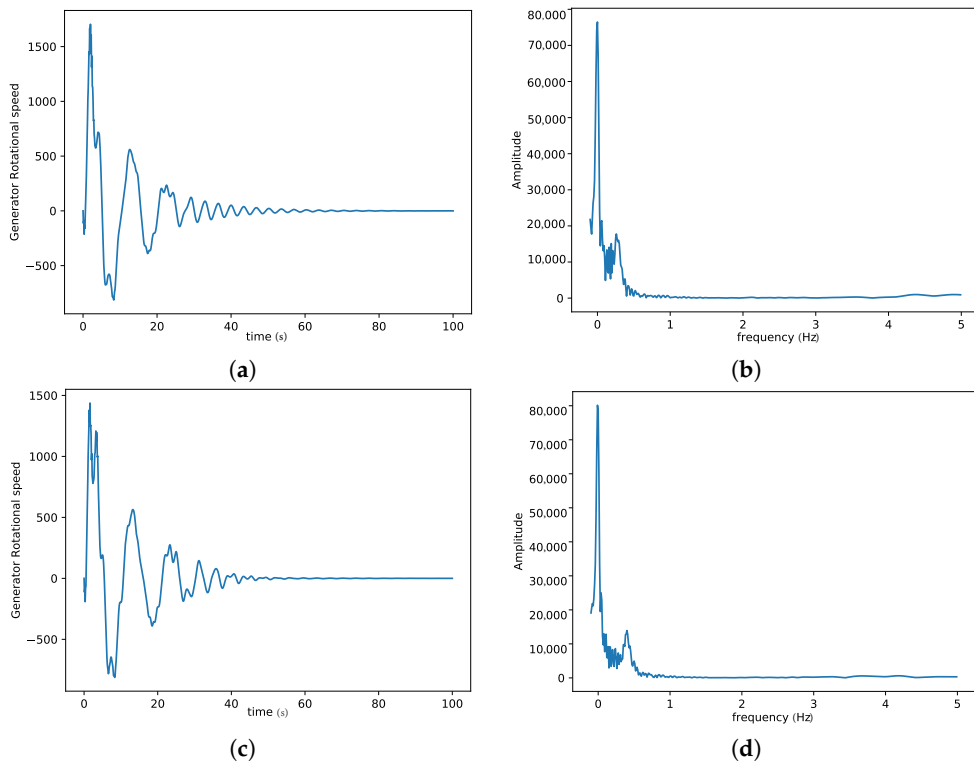


Figure 8. The effect of a bigger helical angle on generator rotational speed ($\dot{\theta}_4$). (a,b) are the time series and the corresponding FFT frequency spectrum plots for the case $\beta = \pi/6$. In (c,d), the helical angle has been set to $\beta = \pi/12$. The other parameters are fixed and listed in Table 2.

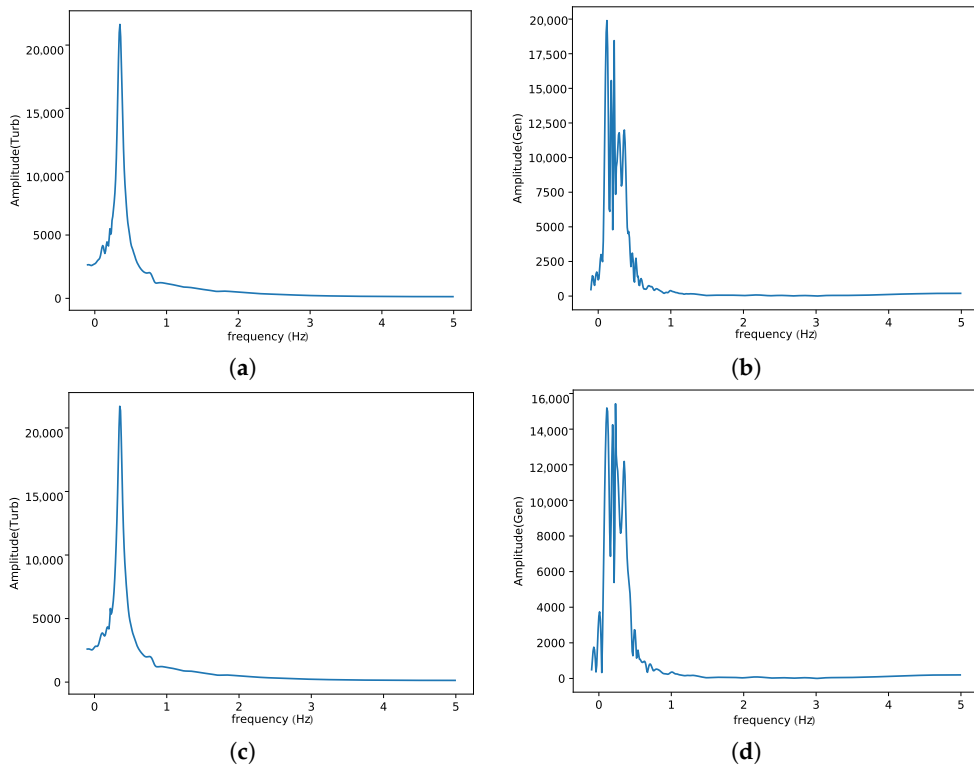


Figure 9. The effect of a smaller mesh frequency on wind turbine and generator rotational speed. (a,b) are the turbine and generator FFT frequency spectrum respectively for $\omega_m = 0.05$. In (c,d), the mesh frequency has been set to $\omega_m = 0.5$. The other parameters used for these plots are presented in Table 2.

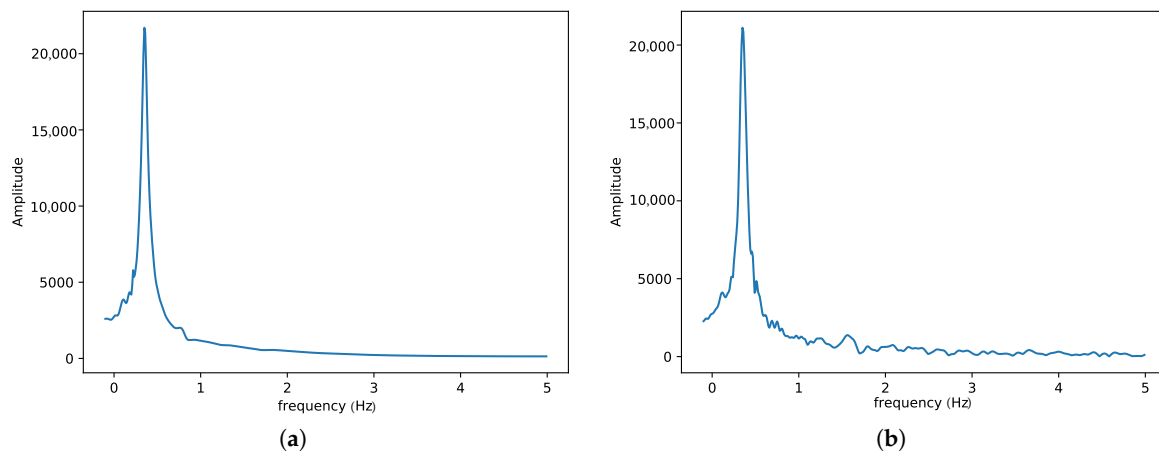


Figure 10. The effect of external excitation frequency on wind turbine rotational speed. (a) is for the case $\omega_i = 0.02$; and (b) is for the case $\omega_i = 0.2$. The other parameters used for these plots are presented in Table 2.

4. Conclusions

To conclude, we have developed a complex nonlinear model for a six-degree-of-freedom (DOF) single-mesh helical gear train by including a time-varying mesh stiffness, axial vibrations, torsional vibrations, shaft and bearing damping, generator back EMF and gear backlashes. With the help of a time series and FFT frequency spectrum, we have studied the effects of these nonlinear terms on the wind turbine and generator rotational speeds under different excitation conditions by numerically integrating the associated equations using the RK4 algorithm. In our results, we have seen that lightly damped oscillations lead to the generation of extra harmonics in the turbine, which is not favorable for quality current generation. Hence, this can be solved at higher damping, torsional and axial stiffness. This means that including shock absorbers during wind turbine gearbox design will go a long way toward reducing noisy vibrations in the gearbox and hence improving the quality of generated current. We have also seen that big helical angles will generally induce heavy nonlinear vibrations, which might lead to tooth separation at the gear stage, and also, very small small helical angles induce noisy dynamics in the generator. Hence, the helical angle should be set to an optimum value for efficient power conversion. Moreover, we have equally seen that a smaller mesh frequency will induce extra noise in the generator, and the external excitation due to wind gust has a greater influence on the nonlinearity of the wind turbine dynamics as compared to the internal excitations due to static transmission errors, time varying mesh stiffness and the generator back EMF.

5. Future Work

In the future, we are looking forward to where the theory presented here can be applied for new small wind turbine gearbox designs using helices instead of tooth/tooth couplings.

Acknowledgments: This work was supported by the government of Canada's International Development Research Centre (IDRC) and within the framework of the AIMS Research for Africa Project (CMMCM2014025S).

Author Contributions: N.A.A. and A.M.D. conceived and designed the experiments; N.A.A. performed the experiments; N.A.A. and E.J. analyzed the data; A.M.D. and E.J. contributed reagents/materials/analysis tools; N.A.A. wrote the paper.

Conflicts of Interest: The authors declare no conflict of interest.

Abbreviations

The following abbreviations are used in this manuscript:

T_t, T_m	the turbine and generator torques
I_i	the moment of inertia of the wheels
m_i	the masses of the wheels
θ_i	the angular positions of the wheels
K_l, K_h, K_2, K_3	the low speed shaft torsional stiffness, high speed shaft torsional stiffness and bearing stiffness for Gear 1 and Gear 2, respectively
C_l, C_h, C_2, C_3	the low speed shaft damping, high speed shaft damping and bearing damping for Gear 1 and Gear 2, respectively
β	the helical or pressure angle
C_m and K_m	the mesh damping and stiffness, respectively
RK4	Runge-Kutta of order 4

References

1. Perdana, A. *Dynamic Models of Wind Turbines. A Contribution towards the Establishment of Standardized Models of Wind Turbines for Power System Stability Studies*; Avancez: Goteborg, Sweden, 2008; pp. 29–32, ISBN 978-91-7385-226-5.
2. Wasynczuk, O.; Man, D.; Sullivan, J. Dynamic behavior of a class of wind turbine generators during random wind fluctuations. *IEEE Trans. Power Syst. Appar. Syst.* **1981**, *PAS-100*, 2837–2845.
3. Hinrichsen, E.; Nolan, P. Dynamics and stability of wind turbine generators. *IEEE Trans. Power Appar. Syst.* **1982**, *101*, 2640–2648.
4. Zhao, M.; Ji, J.C. Nonlinear torsional vibrations of a wind turbine gearbox. *Appl. Math. Modell.* **2015**, *39*, 4928–4950, doi:10.1016/j.apm.2015.03.026.
5. Zhao, M.; Ji, J. Dynamic Analysis of Wind Turbine Gearbox Components. *Energies* **2016**, *9*, 110, doi:10.3390/en9020110.
6. Yang, F.; Shi, Z.; Meng, J. Nonlinear dynamics and load sharing of double-mesh helical gear train. *J. Eng. Sci. Technol. Rev.* **2013**, *6*, 29–34.
7. Helsen, J.; Vanhollebeke, F.; Marrant, B.; Vandepitte, D.; Desmet, W. Multibody modeling of varying complexity for modal behavior analysis of wind turbine gearboxes. *Renew. Energy* **2011**, *36*, 3098–3113.
8. Heege, A.; Betran, J.; Radovic, Y. Fatigue load computation of wind turbine gearboxes by coupled finite element, multi-body system and aerodynamic analysis. *Wind Energy* **2007**, *10*, 395–413.
9. Zhao, X.; Maißer, P.; Wu, J. A new multibody modeling methodology for wind turbine structures using a cardanic joint beam element. *Renew. Energy* **2007**, *32*, 532–546.
10. Kim, T.; Hansen, A.M.; Branner, K. Development of an anisotropic beam finite element for composite wind turbine blades in multibody system. *Renew. Energy* **2013**, *59*, 172–183.
11. Pappalardo, C.M. A natural absolute coordinate formulation for the kinematic and dynamic analysis of rigid multibody systems. *Nonlinear Dyn.* **2015**, *81*, 1841–1869.
12. Pappalardo, C.M.; Guida, D. On the use of two-dimensional Euler parameters for the dynamic simulation of planar rigid multibody systems. *Arch. Appl. Mech.* **2017**, *87*, 1647–1665.
13. Girsang, I.P.; Dhupia, J.S.; Eduard, M.; Mohit, S. Gearbox and Drivetrain Models to Study Dynamic Effects of Modern Wind Turbines. National Renewable Energy Laboratory (NREL). Available online: www.nrel.gov/publications (accessed on 28 February 2018).
14. Parker, R.G.; Lin, J. Mesh phasing relationships in planetary and epicyclic gears. *J. Mech. Des.* **2004**, *126*, 365–370.
15. Masters, G.M. *Renewable and Efficient Electric Power Systems*; John Wiley & Sons: Hoboken, NJ, USA, 2005.

